Influence of ozone recovery and greenhouse gas increases on Southern Hemisphere circulation

Alexey Y. Karpechko,[1,2] Nathan P. Gillett,[3] Lesley J. Gray,[4] and Mauro Dall'Amico[5,6]

Received 27 April 2010; revised 6 September 2010; accepted 13 September 2010; published 24 November 2010.

[1] Stratospheric ozone depletion has significantly influenced the tropospheric circulation and climate of the Southern Hemisphere (SH) over recent decades, the largest trends being detected in summer. These circulation changes include acceleration of the extratropical tropospheric westerly jet on its poleward side and lowered Antarctic sea level pressure. It is therefore expected that ozone changes will continue to influence climate during the 21st century when ozone recovery is expected. Here we use two contrasting future ozone projections from two chemistry-climate models (CCMs) to force 21st century simulations of the HadGEM1 coupled atmosphere-ocean model, along with A1B greenhouse gas (GHG) concentrations, and study the simulated response in the SH circulation. According to several studies, HadGEM1 simulates present tropospheric climate better than the majority of other available models. When forced by the larger ozone recovery trends, HadGEM1 simulates significant deceleration of the tropospheric jet on its poleward side in the upper troposphere in summer, but the trends in the lower troposphere are not significant. In the simulations with the smaller ozone recovery trends the zonal mean zonal wind trends are not significant throughout the troposphere. The response of the SH circulation to GHG concentration increases in HadGEM1 includes an increase in poleward eddy heat flux in the stratosphere and positive sea level pressure trends in southeastern Pacific. The HadGEM1-simulated zonal wind trends are considerably smaller than the trends simulated by the CCMs, both in the stratosphere and in the troposphere, despite the fact that the zonal mean ozone trends are the same between these simulations.

Citation: Karpechko, A. Y., N. P. Gillett, L. J. Gray, and M. Dall'Amico (2010), Influence of ozone recovery and greenhouse gas increases on Southern Hemisphere circulation, *J. Geophys. Res.*, *115*, D22117, doi:10.1029/2010JD014423.

1. Introduction

[2] Antarctic stratospheric ozone depletion caused by anthropogenic halogens significantly contributed to the observed acceleration of the Southern Hemisphere (SH) extratropical tropospheric westerly jet on its poleward side during the last decades of the 20th century [*Kindem and Christiansen*, 2001; *Sexton*, 2001; *Gillett and Thompson*, 2003]. As the release of the ozone depleting substances (ODSs) to the atmosphere slowed following the Montreal protocol, their atmospheric concentration has started to decline [*World Meteorological Organization* (*WMO*), 2007]. It is expected that the removal of anthropogenic ODSs from the atmosphere will lead to the recovery of stratospheric ozone layer by the mid-21st century [e.g., *Eyring et al.*, 2007]. The beginning of ozone recovery may already have been detected [e.g., *Stolarski and Frith*, 2006].

[3] Whether or not ozone recovery will be followed by the reversal of the tropospheric circulation changes remains an open question. *Fyfe et al.* [1999] and *Kushner et al.* [2001] showed that the increase of greenhouse gas (GHG) concentration, which is expected to continue throughout the 21st century, can lead to an acceleration of the SH tropospheric jet and an accompanied positive trend of the Southern Annular Mode (SAM). While during the 20th century both GHG concentration increase and ozone depletion forced the circulation toward a more positive SAM, their effects during the period of ozone recovery will compete with each other. The matter is complicated by the fact that changes in stratospheric temperature and dynamics related to the GHG concentration increases will influence the ozone evolution, and ozone concentrations may not be the same as in the preozone hole period even when the anthropogenic ODSs have been removed from the atmosphere [*Waugh et al.*, 2009a].

[1]Climatic Research Unit, School of Environmental Sciences, University of East Anglia, Norwich, UK.
[2]Now at Arctic Research Unit, Finnish Meteorological Institute, Helsinki, Finland.
[3]Canadian Centre for Climate Modelling and Analysis, Environment Canada, Victoria, British Columbia, Canada.
[4]Climate Directorate, National Centre for Atmospheric Sciences, Meteorology Department, University of Reading, Reading, UK.
[5]Deutsches Zentrum für Luft- und Raumfahrt, Institut für Physik der Atmosphäre, Oberpfaffenhofen, Germany.
[6]Now at Astrium GmbH, Ottobrunn, Germany.

0148-0227/10/2010JD014423

[4] The combined effect of GHG increases and ozone recovery on the SH circulation was first studied by *Shindell and Schmidt* [2004] in an atmosphere-ocean general circulation model (AOGCM) with relatively coarse resolution. In their model the effects of ozone recovery and GHG increases roughly balanced each other resulting in insignificant trends in the tropospheric circulation. Further studies with AOGCMs showed significant positive trends of the SAM in summer [*Arblaster and Meehl*, 2006; *Miller et al.*, 2006], suggesting a dominant influence of the GHG concentration increase. However, future ozone changes in some of these models were obtained from simple regression models based on projected ODSs concentrations [*Stott et al.*, 2006] while some other models suffered from erroneously specified ozone forcing [*Miller et al.*, 2006].

[5] A different perspective is given by coupled chemistry climate models (CCMs). Some CCMs simulate a deceleration of the tropospheric jet stream and a negative SAM trend in summer [*Perlwitz et al.*, 2008; *Son et al.*, 2008, *Waugh et al.*, 2009b], although the spread across the CCMs predictions is large and the most recent CCMVal-2 simulations show no significant jet location trend in the summer on average [*Baldwin et al.*, 2010; *Son et al.*, 2010]. The models used in these studies were run with prescribed sea surface temperatures (SSTs), constraining the possible tropospheric response, although *Sigmond et al.* [2010] did not find significant difference between the SAM response to ozone depletion in a model forced by prescribed SSTs and a model coupled to a full ocean.

[6] The present study is aimed at modeling the SH circulation changes during the period of ozone recovery and is designed to overcome some of the deficiencies identified in the previous studies. In this study we use a high-resolution AOGCM forced by both GHG concentration increases and ozone recovery scenarios based on CCM simulations. We choose a model which, according to several studies, simulates many aspects of present tropospheric climate better than the majority of other available AOGCMs. The model has a fully coupled ocean, which means that its response to an applied forcing is not constrained by prescribed SSTs. To account for uncertainties in future ozone evolution, two contrasting ozone recovery scenarios are considered in addition to the scenario in which no ozone recovery is taking place.

2. Model and Methods

[7] The Hadley Centre global environmental model version 1 (HadGEM1) described by *Martin et al.* [2006], *Ringer et al.* [2006], and *Johns et al.* [2006] is used in this study. The atmospheric component of the model has horizontal resolution of 1.25° latitude by 1.875° longitude and 38 levels from the surface to about 39 km with 16 levels typically located above 300 hPa. The oceanic component of the model has a horizontal resolution of 1° (the meridional resolution is 1° between the poles and 30° latitude, from where it increases smoothly to 1/3° at the equator) and 40 unevenly spaced vertical levels. Several studies [*Miller et al.*, 2006; *Connolley and Bracegirdle*, 2007; *Karpechko et al.*, 2009] have shown that HadGEM1 ranks as one of the best AOGCMs in its simulation of global and Antarctic climates, SAM spatial structure, as well as climate impacts of the SAM across the CMIP3 models used in the IPCC AR4 assessment.

[8] The model is run to simulate climate change from 1 December 1978 to 1 December 2049, which comprises the periods of ozone depletion and recovery. Simulations of the past climate were forced by observed changes in well mixed GHGs, tropospheric and stratospheric ozone, aerosols, land use, solar irradiance and stratospheric volcanic aerosols. Implementation of the forcing, except ozone forcing, is described in detail by *Stott et al.* [2006]. Implementation of ozone forcing is described by *Dall'Amico et al.* [2010a]. In these simulations ozone is prescribed as zonal mean monthly mean values based on satellite observations, instead of the monthly climatology with an imposed linear trend component, as is usually employed in AOGCM experiments. It therefore includes significant interannual variability such as that associated with the Quasi-Biennial Oscillation (QBO) and 11 year solar cycle. The model also implements a relaxation toward the observed QBO in stratospheric winds. The implemented changes result in some improvements of the simulated climate variability and trends as described by *Dall'Amico et al.* [2010a, 2010b]. Altogether six 20 year simulations (1 December 1978 to 1 December 1999), referred to as 'Observed_O3' experiments, are considered in this study, three of which are parts of the 'baseline+ozone+QBO' simulations discussed by *Dall'Amico et al.* [2010a, 2010b] and another three identical simulations that have been conducted at a different computing facility. The end points of the latter three simulations are used as starting points for the scenario simulations.

[9] The scenario simulations include three main experiments, each consisting of three ensemble members covering the period from 1 December 1999 to 1 December 2049. The experiments differ in the prescribed ozone forcing but are identical otherwise. The forcing in these experiments includes GHG concentration increases following the SRES A1B emission scenario and changes in aerosols and land use as described by *Stott et al.* [2006]. The relaxation toward the QBO is not included in these experiments. Scenario ozone fields for two of the experiments are taken from CCM simulations which have been accomplished as a part of the Chemistry-Climate Model Validation (CCMVal-1) activity in support of WMO ozone assessment 2006 [*WMO*, 2007]. The CCM simulations are described in detail by *Eyring et al.* [2007], where they are referred to as REF2 simulations. Ozone outputs of two CCMs, GEOSCCM [*Pawson et al.*, 2008] and CMAM [*Fomichev et al.*, 2007], are used in our experiments referred to as 'GEOSCCM_O3' and 'CMAM_O3', respectively. Like all models these two CCMs have biases; however comparison with observations show that these two CCMs are among the better performing models of those which participated in the CCMVal-1 activity [*Eyring et al.*, 2006; *Waugh and Eyring*, 2008; *Karpechko et al.*, 2010]. GEOSCCM simulates one of the largest while CMAM simulates one of the smallest ozone trends (negative during ozone depletion and positive during ozone recovery) across the CCMVal-1 models [*Eyring et al.*, 2006, 2007; *Karpechko et al.*, 2010]. Analyzing simulations with two contrasting ozone evolutions allows us to better assess uncertainties in future tropospheric climate changes associated with future ozone.

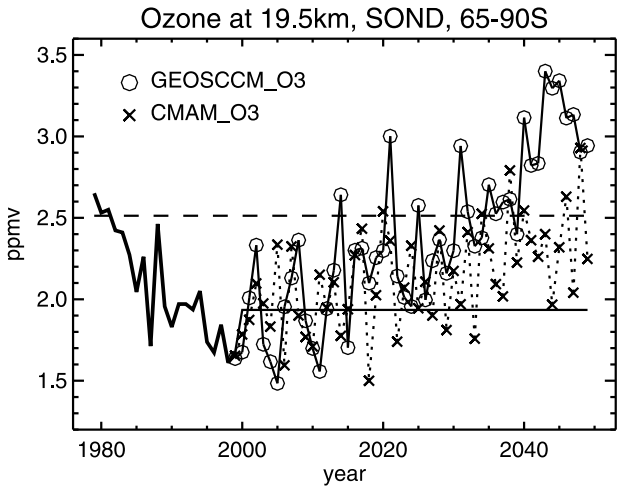

Figure 1. Time series of September–December averaged ozone (ppmv) over the Southern Hemisphere polar cap (65°S–90°S) at 19.5 km used in HadGEM1 simulations. Before 1999 the time series is based on observations (thick solid line). After 1999 they are based on GEOSCCM and CMAM REF2 simulations. Horizontal lines correspond to ozone concentrations used in Constant_O3–2000 (solid line) and Constant_O3–1980 (dashed line) experiments.

[10] Since the background ozone climatology in the two CCMs differ from each other and from the observations, the ozone time series were adjusted by removing the differences between the mean simulated ozone and mean observed ozone averaged over the period of 1998–2003 at each grid point and each month separately. (The GEOSCCM REF2 simulation starts in 2000. The period of averaging for this model is 2000–2004. To start the GEOSCCM_O3 simulations in 1999, GEOSCCM ozone fields from year 2000 were used for both 1999 and 2000 years.) The adjusted time series of October–December mean ozone mixing ratios at 19.5 km (31st model level) over the Antarctic are shown in Figure 1. The trend in CMAM_O3 is a factor 2.5 smaller than that in GEOSCCM_O3. GEOSCCM_O3 Antarctic ozone mixing ratios in 2040–2050 are larger than the observed ones around 1980 because GEOSCCM overestimates background ozone in the lower stratosphere [*Pawson et al.*, 2008], and hence its simulated ozone depletion and recovery is too strong. The observed 1998–2003 climatology is used in the third main experiment referred to as 'Constant_O3–2000.' In this experiment ozone varies only with the annual cycle and is kept constant from year to year. Table 1 provides key information about the experiments.

[11] In addition to the main experiments described above, two sensitivity experiments are performed. To assess the sensitivity of the results to mean ozone climatology, a one-member experiment is performed covering the period from 1 December 1978 to 1 December 2049. Ozone values in this experiment, referred to as 'Constant_O3–1980' are fixed at the observed 1979–1983 mean values. To assess the sensitivity of the results to inclusion of the zonally varying ozone component, a three-member experiment is performed covering the period from 1 December 1999 to 1 December 2049. Ozone fields for this experiment, referred to as 'CMAM_3DO3,' are taken from the CMAM REF2 simulation, as in the CMAM_O3 experiment. But unlike the CMAM_O3 experiment where ozone is prescribed as zonal mean values and is a function of height, latitude, and time only, ozone in CMAM_3DO3 varies also with longitude as simulated by the CMAM model. The motivations for the sensitivity experiments are discussed in section 3.

[12] To reduce the influence of interannual variability on statistics the results of the experiments are presented as ensemble means. The analysis is focused on circulation changes induced by the imposed forcing. The changes are quantified by applying a standard regression model containing a linear trend and allowing for autocorrelation as in work by *Gillett et al.* [2006]. Statistical significance of the ensemble mean trends is estimated using a two-sided *t* test. Our analysis is focused on summer since this is a season when maximal response of the SH circulation to stratospheric ozone changes is expected [*Thompson and Solomon*, 2002].

3. Results

3.1. Zonal Mean Trends

[13] Figure 2 shows seasonal temperature trends over the Antarctic in the past and scenario experiments. The six-member Observed_O3 ensemble average (Figure 2a) shows ozone-induced springtime stratospheric cooling maximizing at about 70 hPa in November. While the timing and the altitude of maximum cooling are in excellent agreement with the observations (not shown), the model underestimates the magnitude of the cooling by about 30% when compared to observations over the comparable period [*Thompson and Solomon*, 2005]. The underestimation may indicate weaknesses of the model's radiation scheme, but may also be due to too weak ozone trends specified. The latter is difficult to verify since ozone observations in the Antarctic stratosphere

Table 1. Description of the Experiments

Name	Number of Simulations in Ensemble	Period	Ozone Forcing	Zonally Asymmetric Ozone
Observed_O3	6	1.12.1978–1.12.1999	Observed	No
Constant_O3–2000	3	1.12.1999–1.12.2049	Fixed at observed 1998–2003 climatology	No
GEOSCCM_O3	3	1.12.1999–1.12.2049	GEOSCCM REF2	No
CMAM_O3	3	1.12.1999–1.12.2049	CMAM REF2	No
CMAM_3DO3	3	1.12.1999–1.12.2049	CMAM REF2	Yes
Constant_O3–1980	1	1.12.1978–1.12.2049	Fixed at observed 1979–1983 climatology	No

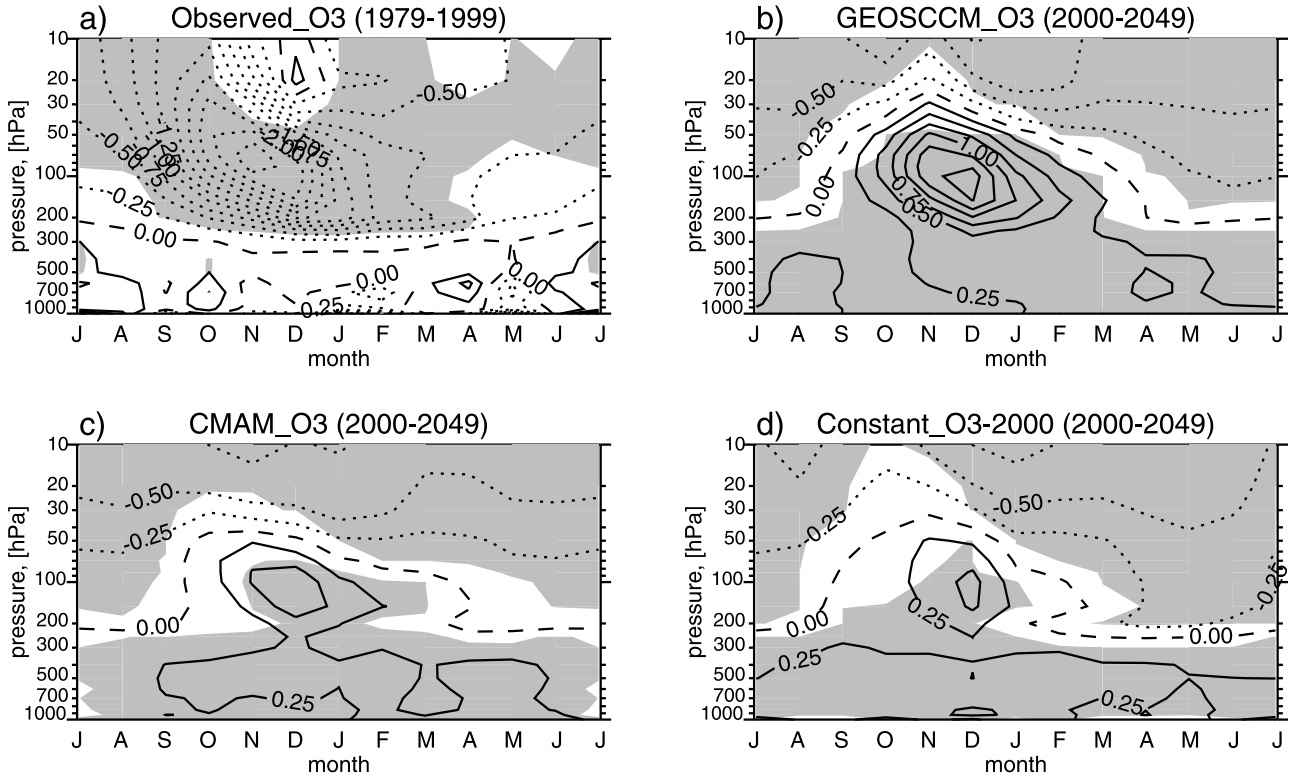

Figure 2. Seasonal cycle of linear trends in temperature (K per decade) over the Southern Hemisphere polar cap (65°S–90°S) in (a) Observed_O3, (b) GEOSCCM_O3, (c) CMAM_O3, and (d) Constant_O3–2000 experiments. Shading denotes trends significant at the 5% level allowing for autocorrelation.

are scarce, which explains why Antarctic ozone trends in observation-based data sets differ significantly [*Karpechko et al.*, 2010]. The data set employed in this study shows the smallest ozone trends during austral spring across the three data sets analyzed by *Karpechko et al.* [2010]. When forced by an ozone data set with larger ozone trends [*Dall'Amico et al.*, 2010a, 2010b], HadGEM1 simulates cooling that is in a good agreement with observations (not shown).

[14] The scenario simulations forced by ozone recovery scenarios reveal warming of the lower stratosphere with a maximum at 100 hPa in December (Figures 2b and 2c). Consistent with the larger ozone trends in the GEOSCCM_O3 simulations, the warming is larger in these simulations than in CMAM_O3. The ratio of warming in GEOSCCM_O3 to that in CMAM_O3 is close to the ratio of the corresponding ozone trends. Statistically significant warming in the lower stratosphere in November–January is also simulated in the Constant_O3–2000 experiment, which is somewhat surprising, given the constant ozone forcing in these simulations. As will be shown below this warming is attributable to the dynamical heating caused by increased planetary wave propagation into the stratosphere associated with increases in GHG concentrations.

[15] Figure 3 shows the zonal mean zonal wind trends in the SH in the past and scenario experiments averaged over December–February. The Observed_O3 simulations (Figure 3a) reproduce the strengthening of the stratospheric winds and the acceleration of the tropospheric jet stream on the polarward side seen in the ERA-40 reanalysis data [*Son et al.*, 2008], although with a smaller magnitude than observed, which is, at least partly, due to the underestimated stratospheric cooling. The poleward shift of the tropospheric jet stream is consistent with a positive SAM trend. Positive trends are also simulated equatorward of 40°S both in the stratosphere and in the troposphere, which are not seen in the ERA-40 reanalysis [*Son et al.*, 2008].

[16] Both ozone recovery experiments reveal a weakening of the stratospheric winds, but this is only significant in GEOSCCM_O3 (Figures 3b and 3c). GEOSCCM_O3 shows an equatorward shift of the tropospheric jet stream at 50°S, with the negative trends at 60°S extending to the surface but not statistically significant below 400 hPa. The jet stream shift is not simulated in CMAM_O3. Significant negative trends in polar stratospheric winds are simulated in Constant_O3–2000 (Figure 3d), which is consistent with the lower stratospheric warming in these simulations. There is also an insignificant deceleration of the tropospheric jet on the poleward side in Constant_O3–2000. The opposite wind trends in the subtropical stratosphere between Constant_O3_2000 and the ozone recovery experiments may be attributed, at least partly, to differential meridional heating due to ozone trends in the ozone recovery experiments, where ozone recovery in the midlatitude stratosphere and a weak ozone depletion in the tropical stratosphere (likely due to intensified meridional circulation in the CCM simulations, not shown) result in an easterly thermal wind trend in the subtropical stratosphere.

[17] Based on previous studies [*Miller et al.*, 2006; *Son et al.*, 2008] it was expected that, in the absence of ozone

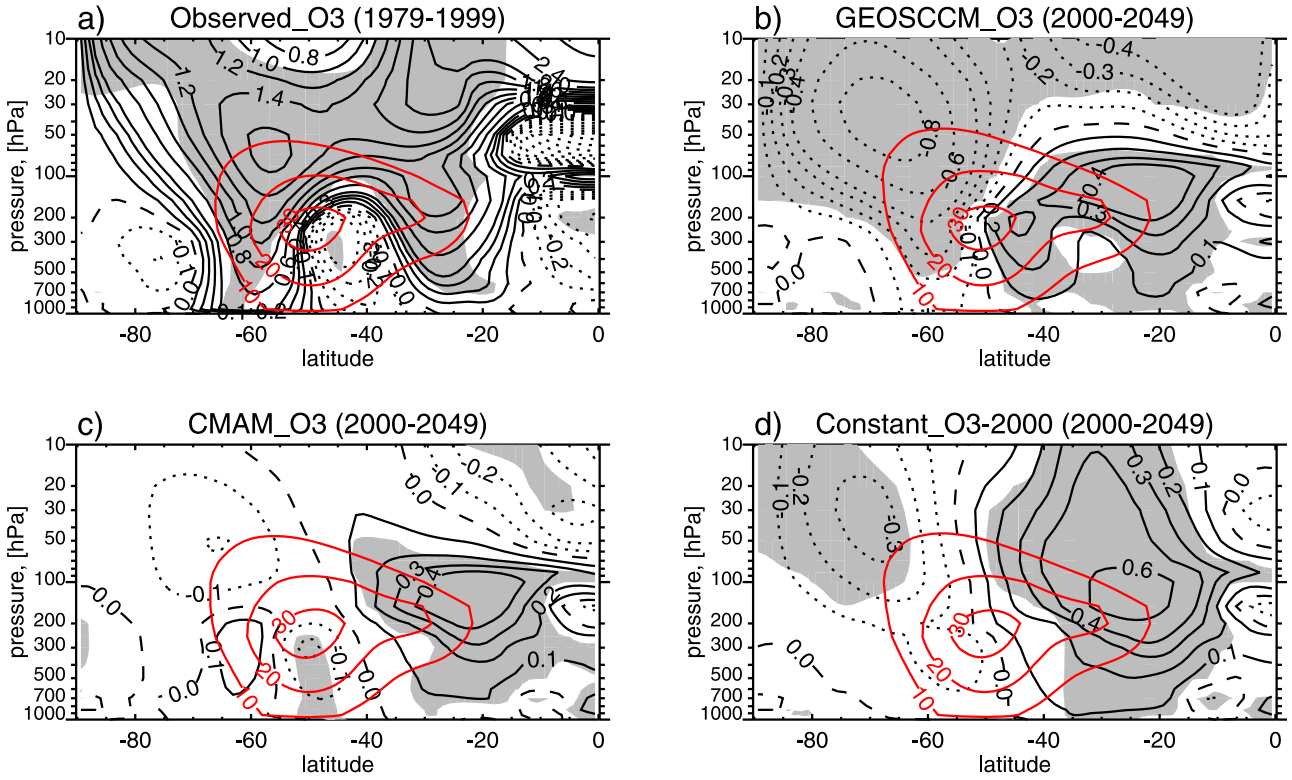

Figure 3. Linear trends in December–February averaged zonal mean zonal winds (m s^{-1} per decade) in the Southern Hemisphere in (a) Observed_O3, (b) GEOSCCM_O3, (c) CMAM_O3, and (d) Constant_O3–2000 experiments. Trend contours are drawn unevenly: each 0.1(0.2) m s^{-1} per decade for absolute values less (more) than 0.4 m s^{-1} per decade. Shading denotes trends significant at the 5% level allowing for autocorrelation. Red contours show climatological mean zonal winds.

recovery, continuing GHG concentration increase will drive a positive SAM trend, further accelerating the tropospheric jet on the poleward side in summer. The reason why it was not simulated in Constant_O3–2000 is likely related to the simulated stratospheric warming (Figure 2d). We find that, in these simulations, detrended October–January mean anomalies of temperature at 100 hPa south of 65°S are significantly negatively correlated ($|r| > 0.4$) with detrended December–February zonal winds at 850 hPa averaged over the 65°S–55°S latitudes, in agreement with previous results [e.g., *Thompson and Solomon*, 2002]. This suggests that the positive stratospheric temperature trends seen in Figure 2d would be associated with negative trends in the tropospheric zonal winds in summer.

[18] Since no radiative forcing (i.e., ozone recovery) that could explain the stratospheric warming was prescribed in these simulations, the explanation is to be sought in induced dynamical changes. It is known that dynamical heating of the polar stratosphere can be induced by enhanced propagation of planetary waves from the troposphere to the stratosphere and associated acceleration of the mean meridional circulation [e.g., *Newman et al.*, 2001]. Figure 4 shows the seasonal trends in zonal mean poleward eddy heat flux $\overline{v'T'}$ at 100 hPa, which is commonly used as a proxy for planetary wave flux into the stratosphere [e.g., *Fusco and Salby*, 1999; *Newman et al.*, 2001]. Figure 4 also shows, for convenience, the climatological values calculated as averages over the whole period. The maximum poleward eddy heat flux is simulated in October–November in all simulations, also in the Observed_O3 experiment (not shown). Comparison with observations [*Hurwitz et al.*, 2010] shows that, while the model captures the timing of the maximum heat flux correctly, the simulated October values are too small. The underestimated heat flux may be related to the extended persistence of the polar vortexes in the model (not shown), which break up about one week later during the period of the Observed_O3 experiment than those in observations during the same period [*Hurwitz et al.*, 2010]. *F. Li et al.* [2010a] suggested that a model with too long persistence of the polar vortexes may unrealistically amplify the ozone recovery effects on climate change in the 21st century.

[19] In both ozone recovery experiments, significant weakening of the poleward eddy heat flux near the latitude of its climatological maximum is simulated in December–January. These trends are related to the shift in time of the final stratospheric warmings which tend to occur earlier as stratospheric ozone recovers (not shown). Following the final warming, the stratospheric westerlies weaken in December–January turning into easterlies in the upper stratosphere, and the mean flow cannot support wave propagation, resulting in a reduction of wave flux into the stratosphere. Although not the main focus of the paper, it is interesting to note that, by 2050, the December–January heat flux values return to the 1980 values in CMAM_O3 and become even smaller in GEOSCCM_O3, evidently following the evolution of

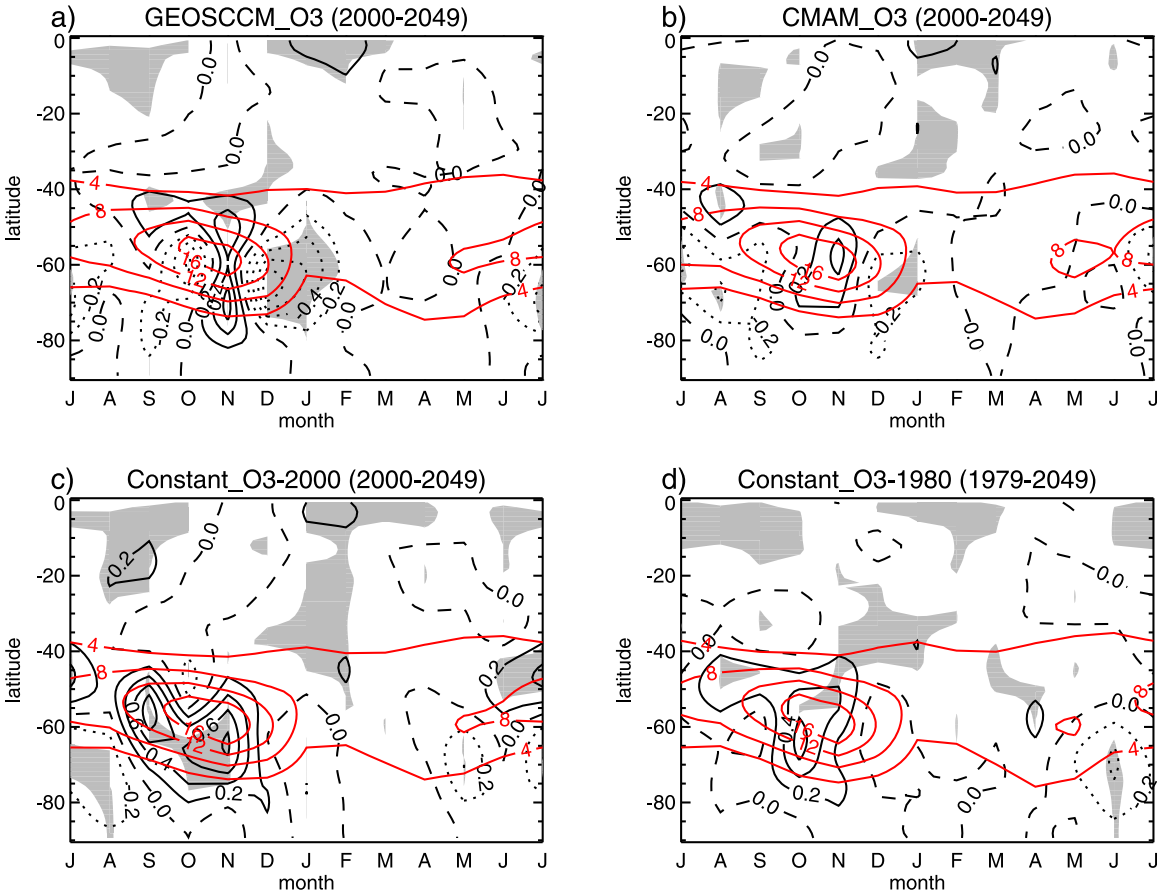

Figure 4. Seasonal cycle of linear trends in eddy heat flux (K m s^{-1} per decade) at 100 hPa in the Southern Hemisphere in (a) GEOSCCM_O3, (b) CMAM_O3, (c) Constant_O3–2000, and (d) Constant_O3–1980 experiments. Shading denotes trends significant at the 5% level allowing for autocorrelation. Red contours show climatological mean eddy heat fluxes. Note that the sign of the fluxes is reversed so that positive values correspond to poleward flux.

stratospheric ozone which is overestimated by 2050 in GEOSCCM_O3 (Figure 1).

[20] In spring, during the time of annual maximum in poleward heat flux, the heat flux trends in the ozone recovery experiments are not significant even when averaged seasonally. However, there is a significant increase in poleward heat flux in spring in Constant_O3–2000, which suggests an acceleration of the mean meridional circulation. This suggestion is supported by calculations of the vertical residual velocity from the EP-flux divergence [*Andrews et al.*, 1987], which show positive trends (increased upwelling) in the tropical stratosphere and negative trends (increased downwelling) in the SH extratropics extending to the South Pole (not shown). *Newman et al.* [2001] showed that polar stratospheric temperatures are influenced by cumulative eddy heat flux into the stratosphere integrated over the preceding months. Figure 5 shows December–January temperatures at 100 hPa averaged south of 65°S when the warming over the Antarctic reaches its maximum, together with results of simple regression model which uses eddy heat flux as a proxy. To obtain these values the September–December mean eddy heat flux averaged south of 45°S was multiplied by the regression coefficient obtained by regression of detrended December–January mean temperature anomalies on the detrended September–December mean eddy heat flux anomalies. The statistical model explains 65% of the warming in Constant_O3–2000, suggesting that the increase of planetary wave flux into the stratosphere is the primary cause of the warming in these simulations. A similar result has also been seen in the Northern Hemisphere under increased GHG scenarios [e.g., *Bell et al.*, 2010]. Figure 5 also shows that the warming in the ozone recovery experiments cannot be explained by heat flux changes alone.

[21] An increased planetary wave flux into the SH stratosphere under ozone hole conditions has previously been reported by *Rind et al.* [2009]. In their model the increase was associated with increased tropospheric eddy kinetic energy, which they attributed to the reduced vertical stability associated with ozone hole cooling. One may speculate that the stratospheric cooling due to increase in GHG concentrations could also lead to the reduced vertical stability, thus explaining the increased wave propagation into the SH stratosphere in the Constant_O3–2000 experiment. To test whether this result depends on prescribed stratospheric ozone concentrations, an additional run, Constant_O3–1980, was performed starting on 1 December 1978 and running through 1 December 2049 with the GHG

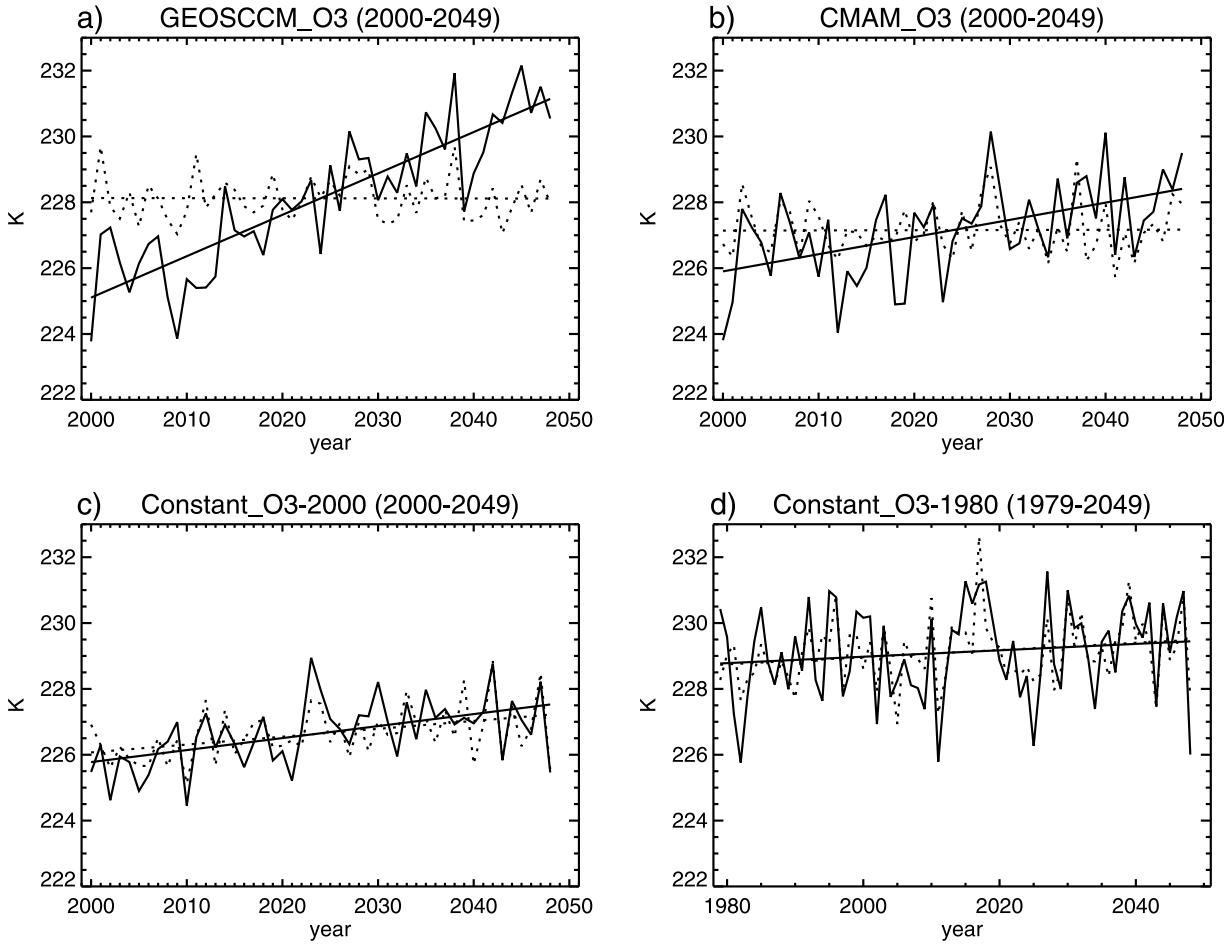

Figure 5. Time series of December–January averaged temperature over the Southern Hemisphere polar cap (65°S–90°S, solid lines) and synthetic temperature based on regression on September–December eddy heat flux averaged over 45°S–90°S (dotted lines) in (a) GEOSCCM_O3, (b) CMAM_O3, (c) Constant_O3–2000, and (d) Constant_O3–1980 experiments. Straight lines show linear trend fits.

forcing identical to that in the past and scenario simulations described above but with ozone concentrations fixed at 1979–1983 mean values (see Figure 1). Figure 4d shows that in Constant_O3–1980 there are positive poleward heat flux trends between August and December with magnitudes somewhat lower than those in the Constant_O3–2000 ensemble mean. The heat flux trend in Constant_O3–1980 is statistically significant at the 5% level when averaged over September–December (Figure 5d). The result suggests that the increase in SH polarward heat flux is a robust response to increased GHG concentrations in HadGEM-1. The magnitude of the heat flux trend in Constant_O3–1980 is only half of the ensemble mean trend in Constant_O3–2000, but one of the three Constant_O3–2000 ensemble members shows a trend of comparable magnitude to that in Constant_O3–1980. Therefore the statistics does not allow us to conclude whether or not the eddy heat flux increase depends on stratospheric ozone concentration. Consistent with the heat flux trend, a lower stratosphere warming is observed in Constant_O3–1980 in late spring and early summer peaking at 0.3K per decade at 100 hPa in November, although it is not statistically significant in either month.

3.2. Surface Trends

[22] *Marshall* [2003] reported a significant positive trend in the SAM in the late 20th century associated with lowered mean sea level pressure (MSLP) over the Antarctic and increased MSLP in midlatitudes. Figure 6 shows mean sea level pressure trends in the past and scenario simulations averaged over December–February. In the Observed_O3 experiment, MSLP decreases over high latitudes (south of 55°S) and increases in the midlatitude belt strongly project on the positive SAM phase, consistent with observations. The scenario experiments (Figures 6b–6d) reveal little annular component, consistent with the absence of significant zonal wind trends near the surface (Figures 3b–3d). Figure 6 shows a strong nonannular component of the future trends in high latitudes dominated by positive pressure trends centered in the southeastern Pacific, north of the Amundsen and Bellingshausen Seas (ABS).

[23] *Neff et al.* [2008] and *Turner et al.* [2009] recently showed that the response of circulation to ozone depletion includes a zonally asymmetric component. *Turner et al.* [2009] found a significant decrease of geopotential height at 500 hPa in austral autumn centered in the southeastern

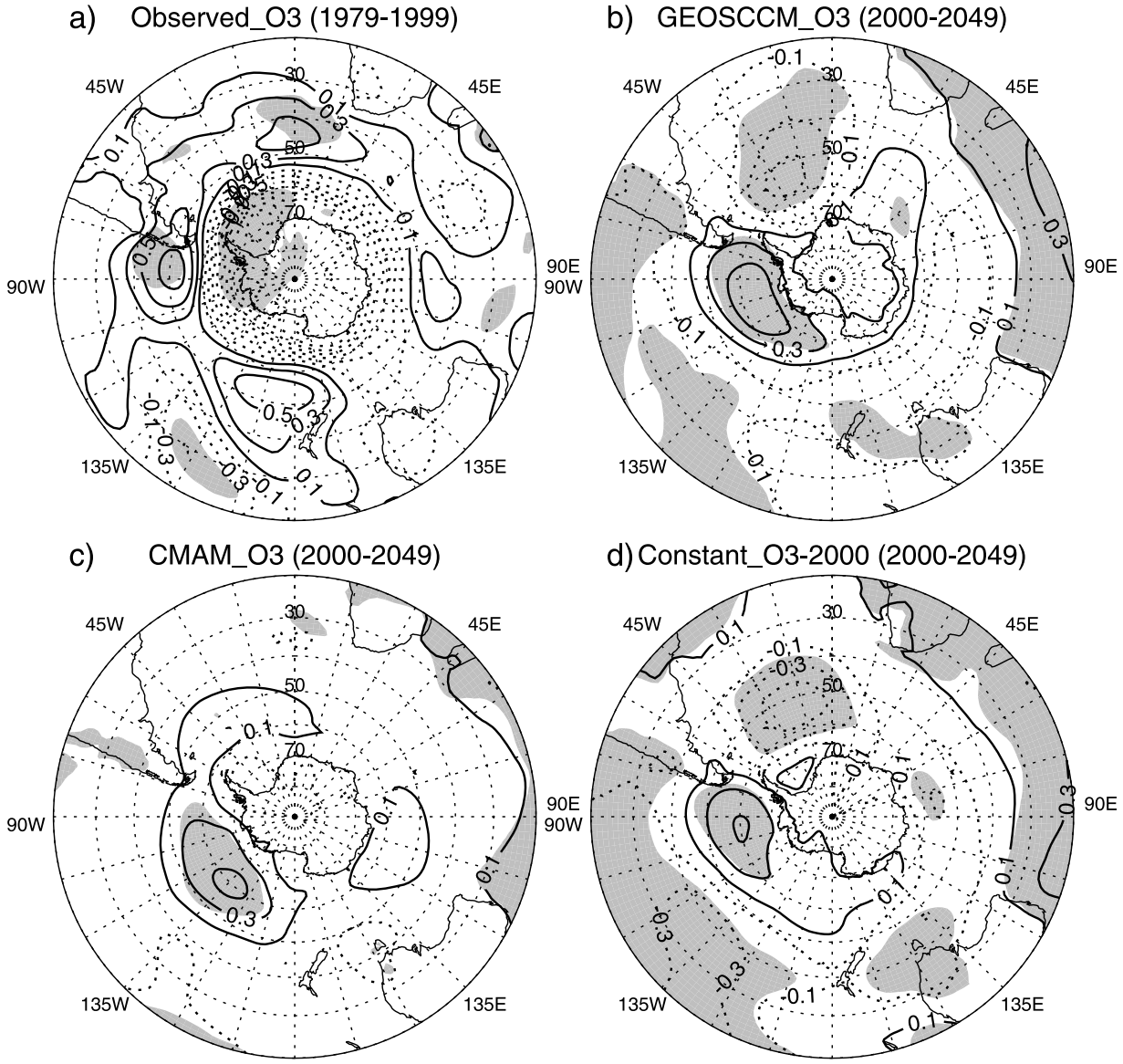

Figure 6. Linear trends in December–February averaged MSLP (hPa per decade) in the Southern Hemisphere in (a) Observed_O3, (b) GEOSCCM_O3, (c) CMAM_O3, and (d) Constant_O3–2000 experiments. Shading denotes trends significant at the 5% level allowing for autocorrelation.

Pacific, although farther south than the positive MSLP trends in Figure 6. To test whether the stratospheric warming contributed to MSLP trends, we calculated the fraction of MSLP trends that is linearly congruent with the trend in November–January mean stratospheric temperatures at 100 hPa south of 65°S. This period is a period of maximum stratospheric warming trends, and a 1 month lead of the stratospheric proxy allows for the downward propagation of the signal to the surface. The linearly congruent trends are calculated at each grid point by, first, regressing the MSLP time series at that grid point on the stratospheric temperature time series and, second, multiplying the resulting regression coefficient by the trend in the stratospheric temperature. To avoid spurious regression due to solely common trends, the regression coefficient is calculated using detrended time series. Figure 7 shows MSLP trends that are linearly congruent with the stratospheric temperature trends, and also the residual trends calculated as a difference between the total MSLP trends and the linearly congruent trends. Not surprisingly the linearly congruent fraction reveals a pronounced SAM signature, and is largest in the GEOSCCM_O3 experiment which has the largest stratospheric warming trend. Comparison of the total trends with the residual trends reveals that the stratospheric warming can only explain a part of the positive MSLP trend in the southeastern Pacific in GEOSCCM_O3 and contributes little to the positive trends in CMAM_O3 and Constant_O3–2000.

[24] Another mode of climate variability that is known to have an influence in the SH high latitudes is El Niño–Southern Oscillation (ENSO). In particular, positive MSLP anomalies appear in summer in high latitudes during El Niño years [*Karoly*, 1989] in association with enhanced blocking in the ABS region [*Renwick*, 1998]. Figure 8 shows the

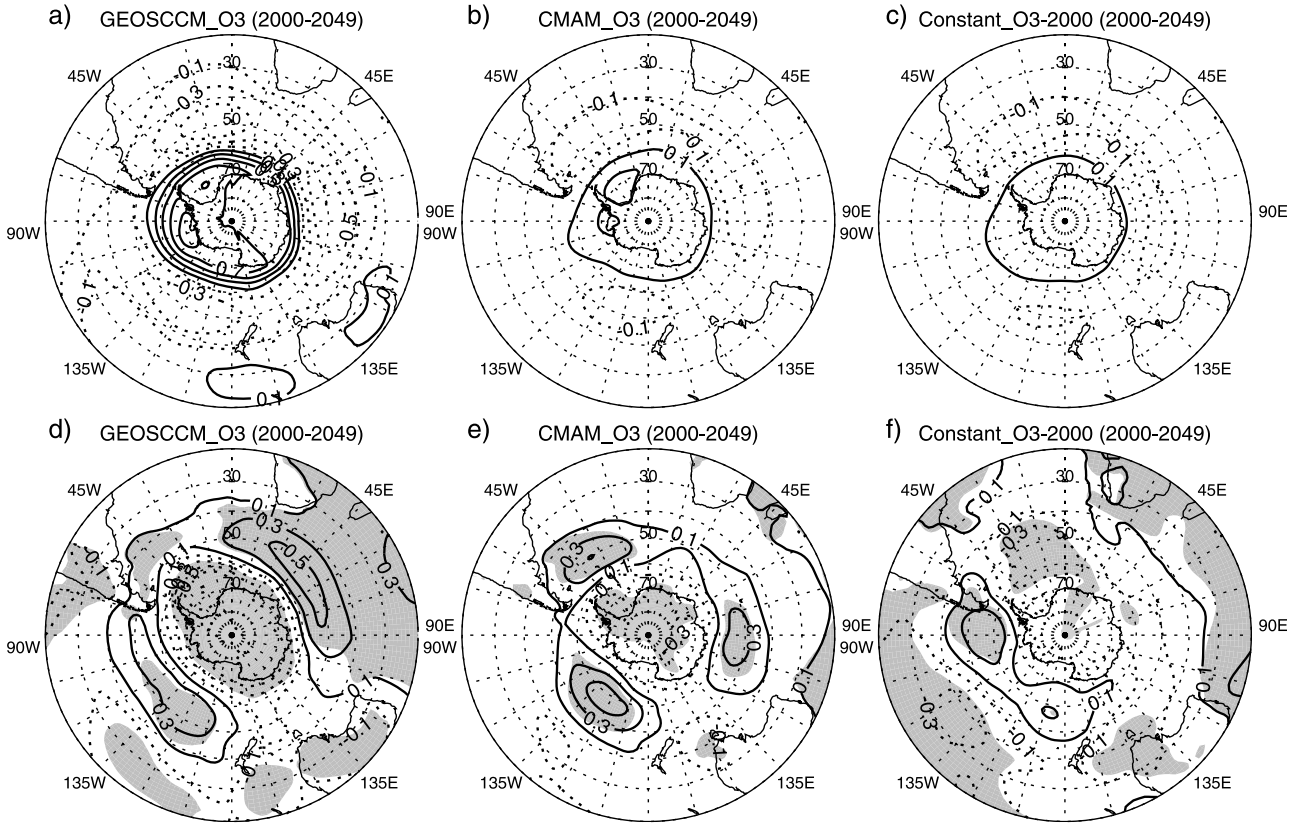

Figure 7. (a, b, c) Trends in December–February averaged MSLP (hPa per decade) in the Southern Hemisphere that are linearly congruent with November–January averaged polar cap temperature trends at 100 hPa and (d, e, f) the residual trends calculated as a difference between the total trends (Figures 6b–6d) and the linearly congruent trends in GEOSCCM_O3 (Figures 7a and 7d), CMAM_O3 (Figures 7b and 7e), and Constant_O3–2000 (Figures 7c and 7f) experiments. Shading in Figures 7d–7f denotes trends significant at the 5% level allowing for autocorrelation.

trends that are linearly congruent with the El Niño 3.4 index used as a proxy of ENSO variability, and the residual trends. In high latitudes, the linearly congruent fraction includes positive trends in the southeastern Pacific, which resemble the total trend patterns and the residual trends in this region are insignificant. We also note that SSTs in the El Niño 3.4 index increase at a similar rate across the experiments.

[25] The link between tropical SSTs and the extratropical circulation anomalies is however complicated. Several authors [e.g., *Harangozo*, 2004; *Grassi et al.*, 2009] showed that the regions of anomalous convection, which triggers the teleconnection pattern in the extratropics by exciting planetary Rossby waves, may not coincide with the area of strongest SST anomalies. *S. Li et al.* [2010] demonstrated that a teleconnection pattern linking tropical Pacific with the extratropics may be triggered by a warming of the tropical Indian Ocean. They speculated that the response in the Pacific may be associated with the Walker cell anomaly linked to the Indian Ocean forcing. Consistent with the findings by *S. Li et al.* [2010], we find that a pattern essentially similar to that shown in Figure 8 can be obtained using the Indian Ocean SSTs averaged over the area used by *S. Li et al.* [2010] (5°S to 5°N, 40°E to 110°E), instead of the El Nino 3.4 index (not shown). Our results therefore strongly suggest that the warming of the tropical oceans contributed to the MSLP changes in high latitudes seen in Figure 6; however it is not possible within our experiments to attribute the extratropical changes to warming in a specific tropical region.

[26] Figure 9 shows comparison of the December–February SAM index evolution in our experiments to that in the multimodel CMIP3 database [*Miller et al.*, 2006; *Son et al.*, 2008]. Following *Miller et al.* [2006] the SAM is defined as the first empirical orthogonal function of MSLP and the SAM index is defined as projection of MSLP on the SAM. The anomalies are calculated with respect to the period 1995–2005, which facilitates comparison of the indexes during the 21st century. Figure 9 shows that our ozone recovery simulations agree well with the CMIP3 simulations, suggesting that the carefully chosen ozone forcing in our experiments does not make a big difference for simulation of the future SAM relative to the previous AOGCM simulations discussed by *Son et al.* [2008]. On the other hand, the Constant_O3_2000 ensemble mean diverges significantly from the corresponding CMIP3 ensemble, which we attribute to the simulated stratospheric dynamical warming in Constant_O3_2000 (see section 3.1).

[27] *Raphael* [2003] reported a significant influence of Antarctic sea ice on the SAM in austral summer; therefore it is also necessary to discuss the evolution of sea ice. In our experiments, December–February mean sea ice area decreases at the average rate of 0.38×10^6 km^2 per decade,

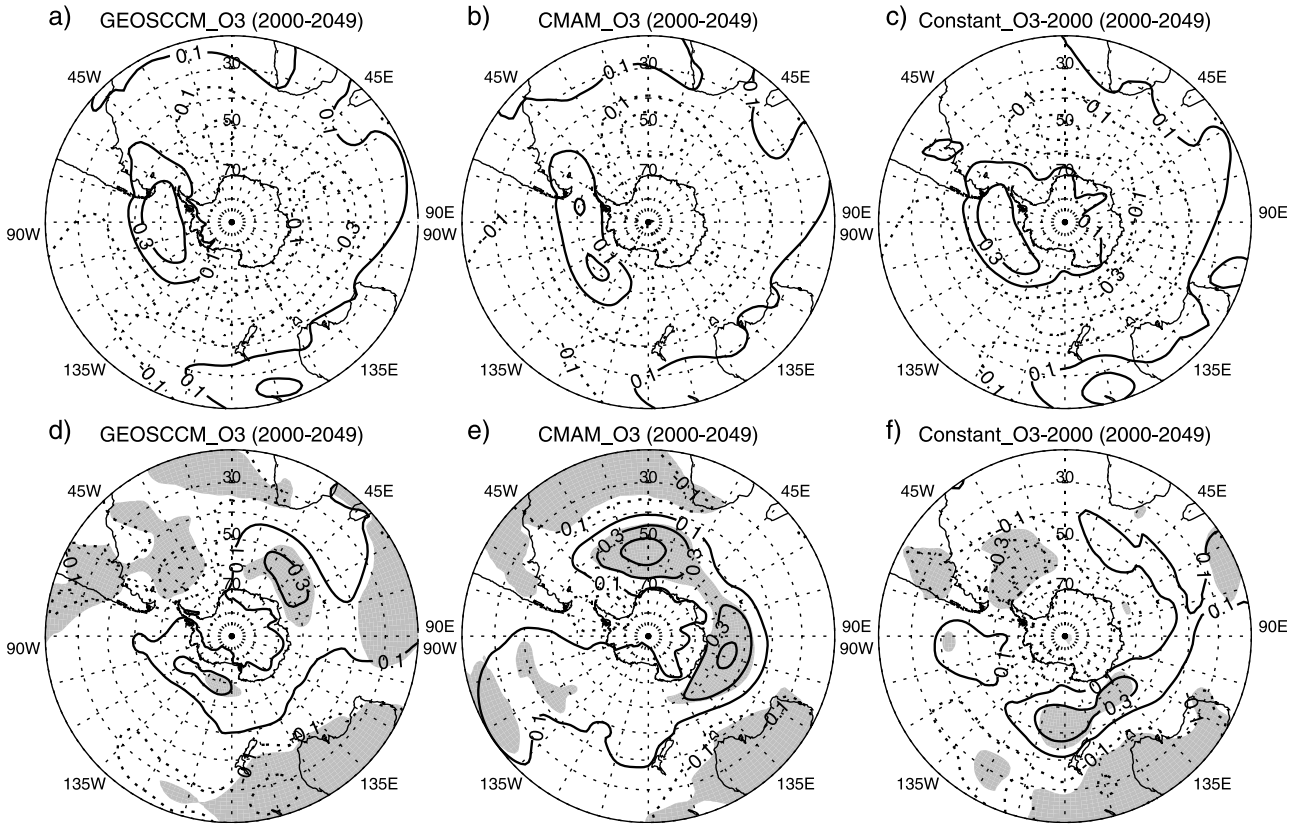

Figure 8. (a, b, c) Trends in December–February averaged MSLP (hPa per decade) in the Southern Hemisphere that are linearly congruent with December–February averaged El Niño 3.4 index trends and (d, e, f) the residual trends calculated as a difference between the total trends (Figures 6b–6d) and the linearly congruent trends in GEOSCCM_O3 (Figures 8a and 8d), CMAM_O3 (Figures 8b and 8e), and Constant_O3–2000 (Figures 8c and 8f) experiments. Shading in Figures 8d–8f denotes trends significant at the 5% level allowing for autocorrelation.

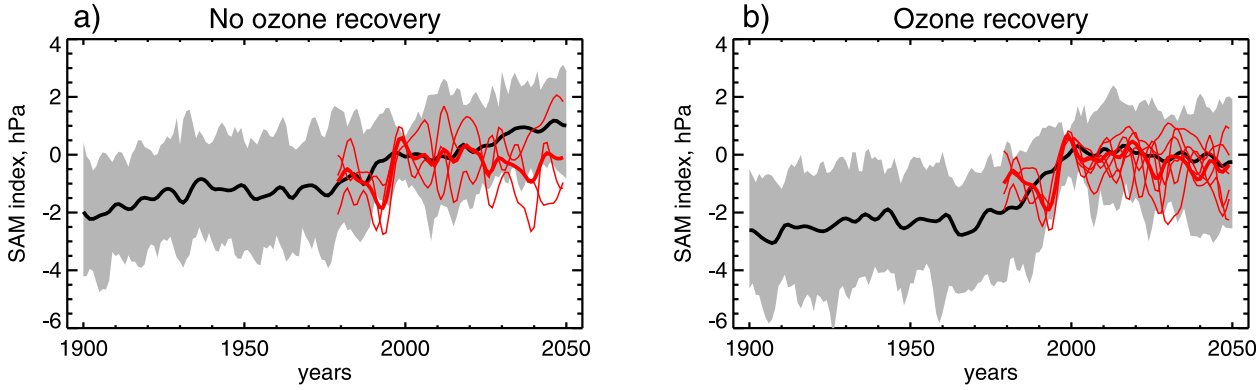

Figure 9. Time series of December–February averaged SAM index (hPa) in the HadGEM1 simulations presented in this paper and in the CMIP-3 multimodel data sets. Shown are anomalies with respect to the period of 1995–2005. (a) CMIP3 models that have no ozone recovery and Constant_O3_2000. (b) CMIP3 models that have ozone recovery, GEOSCCM_O3, and CMAM_O3. Three members of the Observed_O3 ensemble that were continued in the 21st century are shown for convenience in Figures 9a and 9b. Thick black lines show multimodel mean index averaged across individual CMIP3 models; shaded area shows 5 to 95% interval across individual CMIP3 simulations. Individual HadGEM1 simulations are shown with thin red lines, and their average is shown with thick red lines.

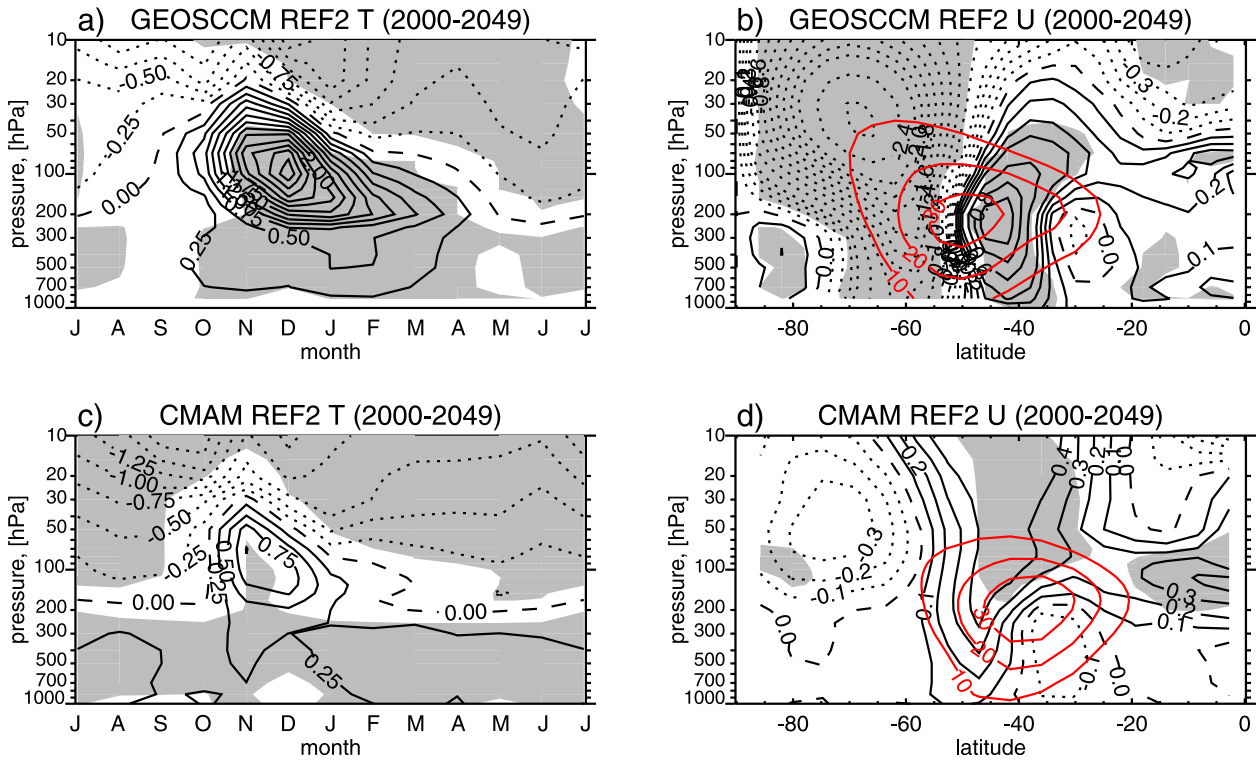

Figure 10. (a, c) Seasonal cycle of linear trends in temperature (K per decade) over the Southern Hemisphere polar cap (65°S–90°S) and (b, d) linear trends in December–February averaged zonal mean zonal winds (m s^{-1} per decade) in the Southern Hemisphere in GEOSCCM REF2 (Figures 10a and 10b) and CMAM REF2 (Figures 10c and 10d) simulations. Trend contours in Figures 10b and 10d are drawn unevenly: each 0.1(0.2) m s^{-1} per decade for absolute values less (more) than 0.4 m s^{-1} per decade. Shading denotes trends significant at the 5% level allowing for autocorrelation. Red contours in Figures 10b and 10d show climatological mean zonal winds.

consistently across the experiments, and constitutes, by the end of the simulations, ~87% of the values at the beginning of the 21st century. According to *Raphael* [2003], a 3% decrease in the sea ice area is sufficient to induce a significant SAM index increase; therefore the effects of the future decreased sea ice oppose to the influence of ozone recovery. However, the lack of positive SAM response in Constant_O3_2000 suggests that the sea ice evolution is not a major driver of the SAM in our experiments.

3.3. Comparison With CCM Simulations

[28] Previous studies showed that while CCMs simulate a significant westerly jet deceleration throughout the troposphere as a response to ozone recovery, AOGCMs typically simulate weaker zonal wind trends that do not reach the surface [*Perlwitz et al.*, 2008; *Son et al.*, 2008]. There are several structural differences between CCMs and AOGCMs. While CCMs include coupled interactive chemistry and extend to the mesosphere or above, thus fully resolving the stratosphere, they generally impose SSTs at the lower boundary. AOGCMs, on the other hand, have a fully coupled ocean but no interactive chemistry and do not fully resolve the stratosphere. Differences in their responses are therefore difficult to attribute. However, one reason for the difference that can be investigated in these simulations might be that the ozone trends in CCMs and in AOGCMs are different. Figure 10 shows seasonal trends in SH polar cap temperatures and December–February averaged trends in SH zonal wind for GEOSCCM and CMAM simulations that provided the ozone fields used in the HadGEM1 GEOSCCM_O3 and CMAM_O3 experiments correspondingly. Despite identical zonal mean ozone trends the CCMs simulate larger stratospheric warming than the corresponding HadGEM-1 experiments (Figures 2b and 2c). Consistently, both CCMs simulate considerably larger (by factor 2–3) negative trends in the extratropical stratospheric winds than HadGEM-1 does (Figures 3b and 3c). CMAM does not simulate deceleration in the tropospheric winds, but the trends in the GEOSCCM simulation are significant and reach the surface, in contrast to the GEOSCCM_O3 experiment.

[29] Recently, attention was drawn to the fact that the simulated response of atmospheric circulation is sensitive to whether ozone is prescribed as a zonal mean or as a zonally asymmetric quantity [*Gabriel et al.*, 2007; *Crook et al.*, 2008; *Gillett et al.*, 2009]. *Waugh et al.* [2009b] showed that a model driven by zonal mean ozone trends underestimates temperature and wind responses when compared to the same model but driven by zonally asymmetric ozone trends. To test whether the differences between the HadGEM-1 experiments and the CCMs may be explained by the lack of zonal asymmetries in ozone fields in HadGEM-1, another experiment, CMAM_3DO3, was performed, in which HadGEM-1 was forced by

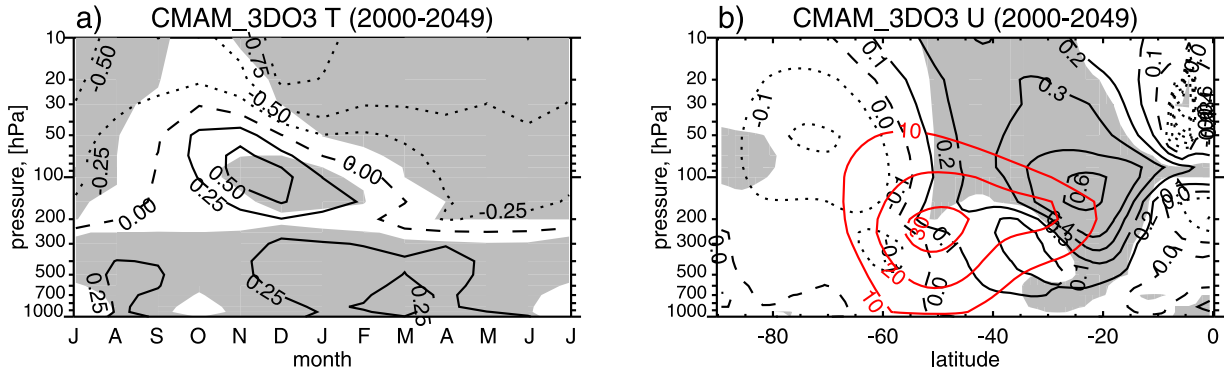

Figure 11. (a) Seasonal cycle of linear trends in temperature (K per decade) over the Southern Hemisphere polar cap (65°S–90°S) and (b) linear trends in December–February averaged zonal mean zonal winds (m s^{-1} per decade) in the Southern Hemisphere in the CMAM_3DO3 experiment. Trend contours in Figure 11b are drawn unevenly: each 0.1 (0.2) m s^{-1} per decade for absolute values less (more) than 0.4 m s^{-1} per decade. Shading denotes trends significant at the 5% level allowing for autocorrelation. Red contours in Figure 11b show climatological mean zonal winds.

three-dimensional (i.e., including zonal asymmetries) monthly mean ozone fields from the CMAM REF2 simulation. Note that zonally averaged ozone fields from CMAM_3DO3 are identical to those in CMAM_O3. Ozone zonal asymmetry in CMAM_3DO3, as represented by the standard deviation around zonal mean value, maximizes over the SH polar cap in November and decreases significantly toward the end of simulations following the ozone hole recovery. By prescribing ozone values, this experiment still misses possible chemistry-climate feedbacks in the stratosphere, which is an important difference from the study by *Waugh et al.* [2009a] which employed a fully coupled chemistry-climate model. However, a qualitative agreement between the result by *Waugh et al.* [2009a] and those by *Crook et al.* [2008] who, similarly to our experiment, used a model with prescribed ozone values, justifies our approach.

[30] Seasonal trends in SH polar cap temperatures and December–February averaged zonal wind trends for CMAM_3DO3 are shown in Figure 11. These plots are very similar to the analogous plots for the CMAM_O3 experiment (Figures 2c and 3c), suggesting that the lack of ozone zonal asymmetry in the HadGEM-1 experiments does not explain the difference with the CCM results.

4. Discussion and Conclusions

[31] Figure 12 illustrates the relationships between lower stratospheric ozone and temperature trends and midtropo-

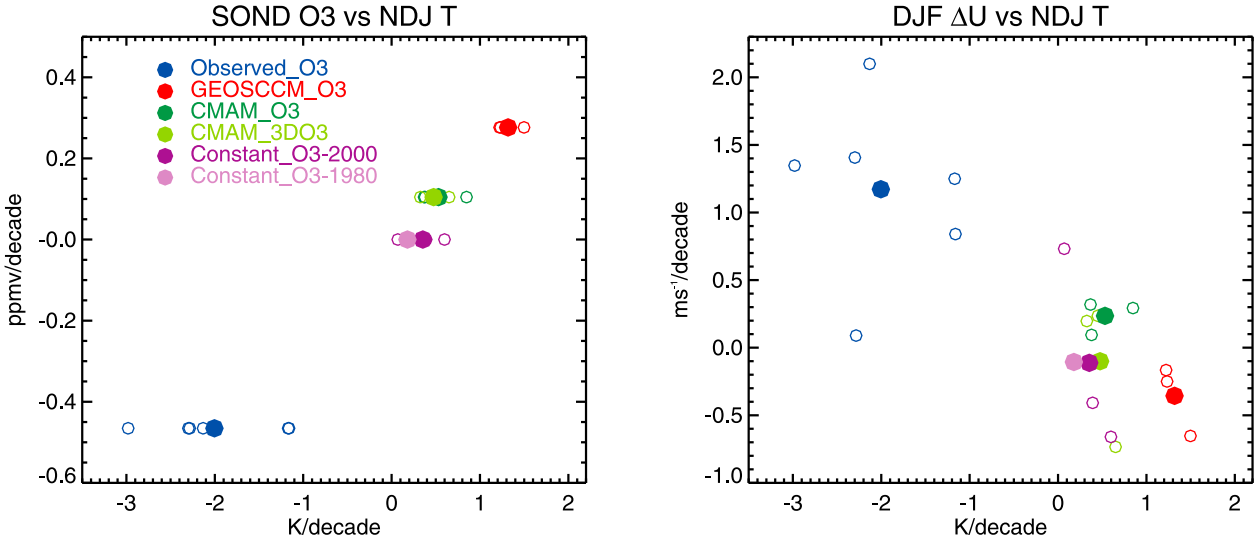

Figure 12. Scatterplots of November–January temperature trends at 100 hPa averaged south of 65°S and (left) September–December ozone mixing ratio at 19.5 km averaged south of 65°S and (right) December–February zonal wind trends at 500 hPa quantified by the difference in zonal winds at 60°S and 45°S. Negative (positive) values of the wind difference denote the deceleration (acceleration) of westerlies on the poleward side of the maximum wind. Ensemble mean values are shown with solid circles; individual members are shown with open circles.

spheric zonal wind trends across the HadGEM1 experiments. Despite considerable internal variability in the tropospheric response to the stratospheric forcing revealed by the spread across the individual ensemble members, our HadGEM1 simulations demonstrate sensitivity of the SH circulation response to ozone recovery trends: larger ozone trends induce a stronger circulation response which projects more strongly on the SAM, consistent with results of *Son et al.* [2008]. However, even when HadGEM1 is forced by ozone recovery trends that are among the largest plausible according to projections by up-to-date CCMs, the simulated response in tropospheric zonal winds is not significant in the lower troposphere, in contrast to the ensemble-mean response across seven CCMs studied by *Son et al.* [2008]. So in our model future SH ozone evolution does not appear to be very important for SH surface climate change. Note that the latest generation of CCMs [*Baldwin et al.*, 2010; *Son et al.*, 2010] also does not show a significant trend in the lower tropospheric winds in the 21st century, in contrast to the previous assessment [*Son et al.*, 2008], but consistent with our results.

[32] Side-by-side comparison with CCMs that have identical ozone trends reveals that HadGEM1 simulates a weaker response in stratospheric temperature and zonal wind than the CCMs. Several factors could be responsible for the difference, including a low upper boundary in HadGEM1, the lack of a dynamical ocean in the CCMs, or more subtle differences between the models. Here we tested a possibility that the different response may be explained by the lack of zonal asymmetries in ozone trends prescribed in HadGEM1. Contrary to several previous studies [*Gabriel et al.*, 2007; *Crook et al.*, 2008; *Gillett et al.*, 2009; *Waugh et al.*, 2009b], we found that the inclusion of zonal asymmetries in ozone does not affect the model's response. One possible explanation for this contradiction may be that in this study we employed a model with a low upper boundary whereas the above studies all used models with upper boundaries located in the mesosphere.

[33] Apart from stratospheric ozone forcing other factors, which are not considered here, can influence the tropospheric response. Differences in the tropospheric zonal wind climatology between HadGEM1 and the CCMs (compare Figures 3 and 10) can lead to different annular responses [*Kidston and Gerber*, 2010; *Son et al.*, 2010]. However, a simple link between the simulated wind climatology and the annular response is difficult to establish in austral summer, when model differences in the treatment of the stratosphere become more important [*Kidston and Gerber*, 2010]. The tropospheric response may also be influenced by differences in model SSTs. However, the influence of different SSTs on the results should be minimal at least in the case of GEOSCCM, since the GEOSCCM simulation is forced by SSTs from the HadGEM1 SRES A1B experiment [*Eyring et al.*, 2007] which has an SST warming pattern similar to our experiments.

[34] We find that HadGEM1 simulates a significant increase in eddy wave flux into the stratosphere in spring as a response to GHG increase similar to those seen in NH studies [e.g., *Bell et al.*, 2010]. The increase leads to a weak lower stratospheric warming over the SH polar cap in late spring–early summer even in simulations without ozone recovery implying a strengthening of the stratospheric meridional circulation in these simulations. The increase in the wave flux is not seen in the simulations where both ozone recovery and GHG increases were prescribed. This suggests that the increased wave flux is associated with changes in vertical wave propagation rather than with changes in wave generation in the troposphere associated with, e.g., increased ocean-land temperature contrast. Since HadGEM1 does not have a well-resolved stratosphere, the simulated changes in the stratospheric meridional circulation should be interpreted with caution and require further investigation, especially taking into account that some models with a well-resolved stratosphere simulate a weakened BD circulation in the Antarctic stratosphere as a response to GHG increases [*McLandress and Shepherd*, 2009].

[35] At the surface our simulations show little annular response in MSLP but instead reveal positive trends centered in southeastern Pacific. The trends appear in all experiments, suggesting that they are a robust response to the GHG concentration increase in HadGEM1. While the trends might be partly attributable to ozone-induced stratospheric warming in some of the simulations, our results also suggest that they are consistent with anomalies expected during El Niño events as a result of teleconnections. *Yamaguchi and Noda* [2006] demonstrated that El Niño–like changes are simulated by the majority of the CMIP3 AOGCM reviewed in the IPCC AR4 assessment, including HadGEM1, during the 21st century as a response to GHG increase. On the other hand, *DiNezio et al.* [2010] argued that the projected changes in the tropical Pacific depart substantially from an ENSO analogy. Further, some studies [e.g., *S. Li et al.*, 2010] demonstrated that the extratropical SH response may also be triggered by the warming in the tropical Indian Ocean, consistent with our calculations. Whether or not the high-latitude MSLP response to the positive trend in the tropical SSTs is a robust response across AOGCM remains to be investigated. The MSLP trends and associated circulation changes in the southeastern Pacific may have important consequences for sea ice distribution [*Stammerjohn et al.*, 2008; *Turner et al.*, 2009].

[36] In this study we have demonstrated the response of the summertime SH circulation to GHG concentration increase and realistic ozone recovery scenarios in a high-resolution AOGCM that was previously shown to be one of the best across the available AOGCM in simulating present tropospheric climate. One of the weaknesses of our model is a relatively low upper boundary (about 39 km), which potentially may influence the planetary wave propagation in the stratosphere and so distort the atmospheric response to imposed ozone trends. We plan to repeat these experiments with a high-top version of the model once it becomes available.

[37] **Acknowledgments.** This work is supported by NERC Project NE/E006787/1. A.K. was also partly supported by Finnish Academy through a personal postdoctoral grant and SAARA project. We acknowledge the GEOSCCM and CMAM modeling groups for making their simulations available for this analysis, the CCMVal activity for WCRP's SPARC project for organizing and coordinating the model data analysis activity, the BADC for collecting and archiving the CCMVal model output, and the Program for Climate Model Diagnosis and Intercomparison (PCMDI) and the WCRP's Working Group on Coupled Modeling (WGCM) for their roles in making available the WCRP CIMP3 multimodel data set. Support of this data set is provided by the Office of Science, U.S. Department of Energy. We thank David Plummer for providing 3-D ozone fields from CMAM simulation, Karen Rosenlof for providing ozone data set, the Met Office for use of HadGEM1, Scott Osprey, Lois Steenman-

Clark, and Jeff Cole for help with running the model, and two anonymous reviewers for constructive comments.

References

Andrews, D. G., J. R. Holton, and C. B. Leovy (1987), *Middle Atmosphere Dynamics*, 489 pp., Academic, San Diego, Calif.

Arblaster, J. M., and G. A. Meehl (2006), Contributions of external forcings to Southern Annular Mode trends, *J. Clim.*, *19*, 2896–2905, doi:10.1175/JCLI3774.1.

Baldwin, M. P., et al. (2010), Effects of the stratosphere on the troposphere, in *SPARC CCMVal Report on the Evaluation of Chemistry-Climate Models*, edited by V. Eyring, T. G. Shepherd, and D. W. Waugh, chap. 10, pp. 379–412, WCRP, Geneva, Switzerland. (Available at http://www.atmosp.physics.utoronto.ca/SPARC/ccmval_final/PDFs_CCMVal%20June%2015/ch10.pdf)

Bell, C. J., L. J. Gray, and J. Kettleborough (2010), Changes in Northern Hemisphere stratospheric variability under increased CO_2 concentrations, *Q. J. R. Meteorol. Soc.*, *136*, 1181–1190, doi:10.1002/qj.633.

Connolley, W. M., and T. J. Bracegirdle (2007), An Antarctic assessment of IPCC AR4 coupled models, *Geophys. Res. Lett.*, *34*, L22505, doi:10.1029/2007GL031648.

Crook, J. A., N. P. Gillett, and S. P. E. Keeley (2008), Sensitivity of Southern Hemisphere climate to zonal asymmetry in ozone, *Geophys. Res. Lett.*, *35*, L07806, doi:10.1029/2007GL032698.

Dall'Amico, M., L. J. Gray, K. H. Rosenlof, A. A. Scaife, K. P. Shine, and P. A. Stott (2010a), Stratospheric temperature trends: Impact of ozone variability and the QBO, *Clim. Dyn.*, *34*, 381–398, doi:10.1007/s00382-009-0604-x.

Dall'Amico, M., P. A. Stott, A. A. Scaife, L. J. Gray, K. H. Rosenlof, and A. Y. Karpechko (2010b), Impact of stratospheric variability on tropospheric climate change, *Clim. Dyn.*, *34*, 399–417, doi:10.1007/s00382-009-0580-1.

DiNezio, P., A. Clement, and G. A. Vecchi (2010), Reconciling differing views of tropical Pacific climate change, *Eos Trans. AGU*, *91*(16), 141–142, doi:10.1029/2010EO160001.

Eyring, V., et al. (2006), Assessment of temperature, trace species, and ozone in chemistry-climate model simulations of the recent past, *J. Geophys. Res.*, *111*, D22308, doi:10.1029/2006JD007327.

Eyring, V., et al. (2007), Multimodel projections of stratospheric ozone in the 21st century, *J. Geophys. Res.*, *112*, D16303, doi:10.1029/2006JD008332.

Fomichev, V. I., et al. (2007), Response of the middle atmosphere to CO_2 doubling: Results from the Canadian Middle Atmosphere Model, *J. Clim.*, *20*, 1121–1144, doi:10.1175/JCLI4030.1.

Fusco, A. C., and M. L. Salby (1999), Interannual variations of total ozone and their relationship to variations of planetary wave activity, *J. Clim.*, *12*, 1619–1629, doi:10.1175/1520-0442(1999)012<1619:IVOTOA>2.0.CO;2.

Fyfe, J. C., G. Boer, and G. Flato (1999), The Arctic and Antarctic oscillations and their projected changes under global warming, *Geophys. Res. Lett.*, *26*, 1601–1604, doi:10.1029/1999GL900317.

Gabriel, A., D. Peters, I. Kirchner, and H.-F. Graf (2007), Effect of zonally asymmetric ozone on stratospheric temperature and planetary wave propagation, *Geophys. Res. Lett.*, *34*, L06807, doi:10.1029/2006GL028998.

Gillett, N. P., and D. W. J. Thompson (2003), Simulation of recent Southern Hemisphere climate change, *Science*, *302*, 273–275, doi:10.1126/science.1087440.

Gillett, N. P., T. D. Kell, and P. D. Jones (2006), Regional climate impacts of the Southern Annular Mode, *Geophys. Res. Lett.*, *33*, L23704, doi:10.1029/2006GL027721.

Gillett, N. P., J. F. Scinocca, D. A. Plummer, and M. C. Reader (2009), Sensitivity of climate to dynamically consistent zonal asymmetries in ozone, *Geophys. Res. Lett.*, *36*, L10809, doi:10.1029/2009GL037246.

Grassi, B., G. Redaelli, and G. Visconti (2009), Evidence for tropical SST influence on Antarctic polar atmospheric dynamics, *Geophys. Res. Lett.*, *36*, L09703, doi:10.1029/2009GL038092.

Harangozo, S. A. (2004), The relationship of Pacific deep tropical convection to the winter and springtime extratropical atmospheric circulation of the South Pacific in El Niño events, *Geophys. Res. Lett.*, *31*, L05206, doi:10.1029/2003GL018667.

Hurwitz, M. M., P. A. Newman, F. Li, L. D. Oman, O. Morgenstern, P. Braesicke, and J. A. Pyle (2010), Assessment of the breakup of the Antarctic polar vortex in two new chemistry-climate models, *J. Geophys. Res.*, *115*, D07105, doi:10.1029/2009JD012788.

Johns, T. C., et al. (2006), The new Hadley Centre climate model (HadGEM1): Evaluation of coupled simulations, *J. Clim.*, *19*, 1327–1353, doi:10.1175/JCLI3712.1.

Karoly, D. J. (1989), Southern Hemisphere circulation features associated with El Niño–Southern Oscillation events, *J. Clim.*, *2*, 1239–1252, doi:10.1175/1520-0442(1989)002<1239:SHCFAW>2.0.CO;2.

Karpechko, A. Y., N. P. Gillett, G. J. Marshall, and J. A. Screen (2009), Climate impacts of the Southern Annular Mode simulated by the CMIP3 models, *J. Clim.*, *22*, 3751–3768, doi:10.1175/2009JCLI2788.1.

Karpechko, A. Y., N. P. Gillett, B. Hassler, K. H. Rosenlof, and E. Rozanov (2010), Quantitative assessment of Southern Hemisphere ozone in chemistry-climate model simulations, *Atmos. Chem. Phys.*, *10*, 1385–1400, doi:10.5194/acp-10-1385-2010.

Kidston, J., and E. P. Gerber (2010), Intermodel variability of the poleward shift of the austral jet stream in the CMIP3 integrations linked to biases in 20th century climatology, *Geophys. Res. Lett.*, *37*, L09708, doi:10.1029/2010GL042873.

Kindem, I. T., and B. Christiansen (2001), Tropospheric response to stratospheric ozone loss, *Geophys. Res. Lett.*, *28*, 1547–1550, doi:10.1029/2000GL012552.

Kushner, P. J., I. M. Held, and T. L. Delworth (2001), Southern Hemisphere atmospheric circulation response to global warming, *J. Clim.*, *14*, 2238–2249, doi:10.1175/1520-0442(2001)014<0001:SHACRT>2.0.CO;2.

Li, F., P. A. Newman, and R. S. Stolarski (2010), Relationships between the Brewer-Dobson circulation and the Southern Annular Mode during austral summer in coupled chemistry-climate model simulations, *J. Geophys. Res.*, *115*, D15106, doi:10.1029/2009JD012876.

Li, S., J. Perlwitz, M. P. Hoerling, and X. Chen (2010), Opposite annular responses of the Northern and Southern Hemisphere to Indian Ocean warming, *J. Clim.*, *23*, 3720–3738, doi:10.1175/2010JCLI3410.1.

Marshall, G. J. (2003), Trends in the Southern Annular Mode from observations and reanalyses, *J. Clim.*, *16*, 4134–4143.

Martin, G. M., M. A. Ringer, V. D. Pope, A. Jones, C. Dearden, and T. J. Hinton (2006), The Physical properties of the atmosphere in the new Hadley Centre global environmental model (HadGEM1). Part I: Model description and global climatology, *J. Clim.*, *19*, 1274–1301, doi:10.1175/JCLI3636.1.

McLandress, C., and T. G. Shepherd (2009), Simulated anthropogenic changes in the Brewer-Dobson circulation, including its extension to high latitudes, *J. Clim.*, *22*, 1516–1540, doi:10.1175/2008JCLI2679.1.

Miller, R. L., G. A. Schmidt, and D. T. Shindell (2006), Forced annular variations in the 20th century Intergovernmental Panel on Climate Change Fourth Assessment Report models, *J. Geophys. Res.*, *111*, D18101, doi:10.1029/2005JD006323.

Neff, W., J. Perlwitz, and M. Hoerling (2008), Observational evidence for asymmetric changes in tropospheric heights over Antarctica on decadal time scales, *Geophys. Res. Lett.*, *35*, L18703, doi:10.1029/2008GL035074.

Newman, P. A., E. R. Nash, and J. E. Rosenfield (2001), What controls the temperature of the Arctic stratosphere during the spring?, *J. Geophys. Res.*, *106*, 19,999–20,010, doi:10.1029/2000JD000061.

Pawson, S., R. S. Stolarski, A. R. Douglass, P. A. Newman, J. E. Nielsen, S. M. Frith, and M. L. Gupta (2008), Goddard Earth Observing System chemistry-climate model simulations of stratospheric ozone-temperature coupling between 1950 and 2005, *J. Geophys. Res.*, *113*, D12103, doi:10.1029/2007JD009511.

Perlwitz, J., S. Pawson, R. L. Fogt, J. E. Nielsen, and W. D. Neff (2008), Impact of stratospheric ozone hole recovery on Antarctic climate, *Geophys. Res. Lett.*, *35*, L08714, doi:10.1029/2008GL033317.

Raphael, M. N. (2003), Impact of observed sea-ice concentration on the Southern Hemisphere extratropical atmospheric circulation in summer, *J. Geophys. Res.*, *108*(D22), 4687, doi:10.1029/2002JD003308.

Renwick, J. A. (1998), ENSO-related variability in the frequency of South Pacific blocking, *Mon. Weather Rev.*, *126*, 3117–3123, doi:10.1175/1520-0493(1998)126<3117:ERVITF>2.0.CO;2.

Rind, D., J. Jonas, S. Stammerjohn, and P. Lonergan (2009), The Antarctic ozone hole and the Northern Annular Mode: A stratospheric interhemispheric connection, *Geophys. Res. Lett.*, *36*, L09818, doi:10.1029/2009GL037866.

Ringer, M. A., et al. (2006), The physical properties of the atmosphere in the New Hadley Centre global atmospheric model (HadGEM1), Part II: Global variability and regional climate, *J. Clim.*, *19*, 1302–1326, doi:10.1175/JCLI3713.1.

Sexton, D. M. H. (2001), The effect of stratospheric ozone depletion on the phase of the Antarctic Oscillation, *Geophys. Res. Lett.*, *28*(19), 3697–3700, doi:10.1029/2001GL013376.

Shindell, D. T., and G. A. Schmidt (2004), Southern Hemisphere climate response to ozone changes and greenhouse gas increases, *Geophys. Res. Lett.*, *31*, L18209, doi:10.1029/2004GL020724.

Sigmond, M., J. C. Fyfe, and J. F. Scinocca (2010), Does the ocean impact the atmospheric response to stratospheric ozone depletion?, *Geophys. Res. Lett.*, *37*, L12706, doi:10.1029/2010GL043773.

Son, S.-W., L. M. Polvani, D. W. Waugh, H. Akiyoshi, R. Garcia, D. Kinnison, S. Pawson, E. Rozanov, T. G. Shepherd, and K. Shibata (2008), The impact of stratospheric ozone recovery on the Southern

Hemisphere westerly jet, *Science*, *320*, 1486–1489, doi:10.1126/science.1155939.

Son, S.-W., et al. (2010), Impact of stratospheric ozone on Southern Hemisphere circulation change: A multimodel assessment, *J. Geophys. Res.*, *115*, D00M07, doi:10.1029/2010JD014271.

Stammerjohn, S. E., D. G. Martinson, R. C. Smith, X. Yuan, and D. Rind (2008), Trends in Antarctic annual sea ice retreat and advance and their relation to El Niño–Southern Oscillation and Southern Annular Mode variability, *J. Geophys. Res.*, *113*, C03S90, doi:10.1029/2007JC004269.

Stolarski, R. S., and S. M. Frith (2006), Search for evidence of trend slowdown in the long-term TOMS/SBUV total ozone data record: The importance of instrument drift uncertainty, *Atmos. Chem. Phys.*, *6*, 4057–4065, doi:10.5194/acp-6-4057-2006.

Stott, P. A., G. S. Jones, J. A. Lowe, P. Thorne, C. Durman, T. C. Johns, and J.-C. Thelen (2006), Transient climate simulations with the HadGEM1 climate model: Causes of past warming and future climate change, *J. Clim.*, *19*, 2763–2782, doi:10.1175/JCLI3731.1.

Thompson, D. W. J., and S. Solomon (2002), Interpretation of recent Southern Hemisphere climate change, *Science*, *296*, 895–899, doi:10.1126/science.1069270.

Thompson, D. W. J., and S. Solomon (2005), Recent stratospheric climate trends: Global structure and tropospheric linkages, *J. Clim.*, *18*, 4785–4795, doi:10.1175/JCLI3585.1.

Turner, J., J. C. Comiso, G. J. Marshall, T. A. Lachlan-Cope, T. Bracegirdle, T. Maksym, M. P. Meredith, Z. Wang, and A. Orr (2009), Non-annular atmospheric circulation change induced by stratospheric ozone depletion and its role in the recent increase of Antarctic sea ice extent, *Geophys. Res. Lett.*, *36*, L08502, doi:10.1029/2009GL037524.

Waugh, D. W., and V. Eyring (2008), Quantitative performance metrics for stratospheric-resolving chemistry-climate models, *Atmos. Chem. Phys.*, *8*, 5699–5713, doi:10.5194/acp-8-5699-2008.

Waugh, D. W., L. Oman, S. R. Kawa, R. S. Stolarski, S. Pawson, A. R. Douglass, P. A. Newman, and J. E. Nielsen (2009a), Impacts of climate change on stratospheric ozone recovery, *Geophys. Res. Lett.*, *36*, L03805, doi:10.1029/2008GL036223.

Waugh, D. W., L. Oman, P. A. Newman, R. S. Stolarski, S. Pawson, J. E. Nielsen, and J. Perlwitz (2009b), Effect of zonal asymmetries in stratospheric ozone on simulated Southern Hemisphere climate trends, *Geophys. Res. Lett.*, *36*, L18701, doi:10.1029/2009GL040419.

World Meteorological Organization (WMO) (2007), Scientific Assessment of Ozone Depletion: 2006, *Global Ozone Res. and Monit. Proj. Rep.*, *50*, Geneva, Switzerland.

Yamaguchi, K., and A. Noda (2006), Global warming patterns over the North Pacific: ENSO vs AO, *J. Meteorol. Soc. Jpn.*, *84*, 221–241, doi:10.2151/jmsj.84.221.

M. Dall'Amico, Astrium GmbH, D-85521, Ottobrunn, Germany.

N. P. Gillett, Canadian Centre for Climate Modelling and Analysis, Environment Canada, Victoria, BC V8W 3V6, Canada.

L. J. Gray, Climate Directorate, National Centre for Atmospheric Sciences, Meteorology Department, University of Reading, Reading RG6 6BB, UK.

A. Y. Karpechko, Arctic Research Unit, Finnish Meteorological Institute, PO Box 503, FI-00101 Helsinki, Finland. (alexey.karpechko@fmi.fi)